

Microscopic understanding of the in-plane thermal transport properties of 2H transition metal dichalcogenides

Citation for published version (APA):

Farris, R., Hellman, O., Zanolli, Z., Saleta Reig, D., Varghese, S., Ordejón, P., Tielrooij, K. J., & Verstraete, M. J. (2024). Microscopic understanding of the in-plane thermal transport properties of 2H transition metal dichalcogenides. *Physical Review B*, 109(12), Article 125422. <https://doi.org/10.1103/PhysRevB.109.125422>

Document license:

CC BY

DOI:

[10.1103/PhysRevB.109.125422](https://doi.org/10.1103/PhysRevB.109.125422)

Document status and date:

Published: 15/03/2024

Document Version:

Publisher's PDF, also known as Version of Record (includes final page, issue and volume numbers)

Please check the document version of this publication:

- A submitted manuscript is the version of the article upon submission and before peer-review. There can be important differences between the submitted version and the official published version of record. People interested in the research are advised to contact the author for the final version of the publication, or visit the DOI to the publisher's website.
- The final author version and the galley proof are versions of the publication after peer review.
- The final published version features the final layout of the paper including the volume, issue and page numbers.

[Link to publication](#)

General rights

Copyright and moral rights for the publications made accessible in the public portal are retained by the authors and/or other copyright owners and it is a condition of accessing publications that users recognise and abide by the legal requirements associated with these rights.

- Users may download and print one copy of any publication from the public portal for the purpose of private study or research.
- You may not further distribute the material or use it for any profit-making activity or commercial gain
- You may freely distribute the URL identifying the publication in the public portal.

If the publication is distributed under the terms of Article 25fa of the Dutch Copyright Act, indicated by the "Taverne" license above, please follow below link for the End User Agreement:

www.tue.nl/taverne

Take down policy

If you believe that this document breaches copyright please contact us at:

openaccess@tue.nl

providing details and we will investigate your claim.

Microscopic understanding of the in-plane thermal transport properties of 2H transition metal dichalcogenides

Roberta Farris ^{1,*} Olle Hellman,² Zeila Zanolli ³ David Saleta Reig ^{1,4} Sebin Varghese ^{1,4} Pablo Ordejón ¹
Klaas-Jan Tielrooij ^{1,4} and Matthieu Jean Verstraete ^{5,6}

¹Catalan Institute of Nanoscience and Nanotechnology - ICN2 (BIST and CSIC), Campus UAB, 08193 Bellaterra (Barcelona), Spain


²Department of Molecular Chemistry and Materials Science, Weizmann Institute of Science, Rehovot 7610001, Israel

³Chemistry Department, Debye Institute for Nanomaterials Science, Condensed Matter and Interfaces, Utrecht University, PO Box 80.000, 3508 TA Utrecht, The Netherlands

⁴Department of Applied Physics, TU Eindhoven, Den Dolech 2, 5612 AZ Eindhoven, The Netherlands

⁵Nanomat/Q-mat/CESAM, Department of Physics, Université de Liège, and European Theoretical Spectroscopy Facility, B-4000 Sart Tilman, Liège, Belgium

⁶Physics Department, ITP Utrecht University, 3508 TA Utrecht, The Netherlands

 (Received 30 October 2023; revised 16 February 2024; accepted 1 March 2024; published 20 March 2024)

Transition metal dichalcogenides (TMDs) are a class of layered materials that hold great promise for a wide range of applications. Their practical use can be limited by their thermal transport properties, which have proven challenging to determine accurately, both from a theoretical and experimental perspective. We have conducted a thorough theoretical investigation of the thermal conductivity of four common TMDs, MoSe₂, WSe₂, MoS₂, and WS₂, at room temperature, to determine the key factors that influence their thermal behavior. We analyze these materials using *ab initio* calculations performed with the SIESTA program, anharmonic lattice dynamics and the Boltzmann transport equation formalism, as implemented in the temperature-dependent effective potentials method. Within this framework, we analyze the microscopic parameters influencing the thermal conductivity, such as the phonon dispersion and the phonon lifetimes. The aim is to precisely identify the origin of differences in thermal conductivity among these canonical TMD materials. We compare their in-plane thermal properties in monolayer and bulk form, and we analyze how the thickness and the chemical composition affect the thermal transport behavior. We showcase how bonding and the crystal structure influence the thermal properties by comparing the TMDs with silicon, reporting the cases of bulk silicon and monolayer silicene. We find that the interlayer bond type (covalent vs. van der Waals) involved in the structure is crucial in the heat transport. In two-dimensional silicene, we observe a reduction by a factor ~ 15 compared to the Si bulk thermal conductivity due to the smaller group velocities and shorter phonon lifetimes. In the TMDs, where the group velocities and the phonon bands do not vary significantly passing from the bulk to the monolayer limit, we do not see as strong a decrease in the thermal conductivity: only a factor 2–3. Moreover, our analysis reveals that differences in the thermal conductivity arise from variations in atomic species, bond strengths, and phonon lifetimes. These factors are closely interconnected and collectively impact the overall thermal conductivity. We inspect each of them separately and explain how they influence the heat transport. We also study artificial TMDs with modified masses, in order to assess how the chemistry of the compounds modifies the microscopic quantities and thus the thermal conductivity.

DOI: [10.1103/PhysRevB.109.125422](https://doi.org/10.1103/PhysRevB.109.125422)

I. INTRODUCTION

Two-dimensional (2D) materials have received significant attention over the past decades due to their potential for applications in electronic and optoelectronic devices [1]. Many new materials have been identified and synthesized, providing ample opportunities for exploring novel physics. A salient

example is the family of transition metal dichalcogenides (TMDs), which show tunable electronic properties depending on the number of layers, transitioning from direct to indirect band gap semiconductors when passing from a 2D monolayer to a 3D bulk crystal [2]. These materials have already yielded prototype applications, in optoelectronics, bio and chemical sensing, flexible electronics, thermoelectrics, and heat management [3]. A crucial aspect in the performance of (opto)electronic devices is their thermal management, to ensure that the systems can operate at reasonable temperatures, and avoid degradation.

In insulators and semiconductors, the thermal conductivity is predominantly governed by quantized lattice vibrations (phonons). Phonons change with the atomic structure, system size, and atomic species involved, leading to a

*roberta.farris@icn2.cat

Published by the American Physical Society under the terms of the [Creative Commons Attribution 4.0 International](https://creativecommons.org/licenses/by/4.0/) license. Further distribution of this work must maintain attribution to the author(s) and the published article's title, journal citation, and DOI.

material-dependent thermal behavior. The thermal conductivity is determined by the efficiency of phonons in transporting heat through several key factors, including their frequency and velocity; their modal heat capacity, which governs how much heat they will carry at a given temperature; their mean-free path (MFP), which reflects how far they can travel before scattering; and the related lifetime, which reflects how long they persist before being absorbed, diffused, or annihilated. Several sources of phonon scattering are relevant for the determination of these properties [4–7]. Resistive scattering between phonons (both normal and Umklapp) due to anharmonic coupling becomes more significant as the temperature increases, leading to a decrease in thermal conductivity. Phonons can also interact with defects (including isotope disorder), surfaces, grain boundaries, and impurities in the lattice, resulting in additional scattering events that reduce the thermal conductivity, which are dominant at low temperatures. The total thermal conductivity of a material depends on the complex interplay between these types of scattering events, including both intrinsic and extrinsic factors. By understanding and controlling these factors, one can design new materials with tailored thermal properties for a wide range of applications and engineer heat transport in devices, to efficiently manage heat and prevent malfunctioning or degradation.

Previous computational studies have predicted the in-plane lattice thermal conductivity, κ_l , of monolayer and bulk TMDs using different approaches. Taking monolayer MoS₂ as an example, this material has been studied using nonequilibrium molecular dynamics (NEMD) [8], the *ab initio* Peierls-Boltzmann equation, the semiempirical Slack equation [9], and the nonequilibrium Green's function (NEGF) [10] formalism, with computed values spreading over two orders of magnitude [11–23]. Even when employing the same approach, there are still unexplained discrepancies in the resulting κ_l values found in the literature. For instance, again in MoS₂, values from 1.35–530 W/m/K have been reported from classical MD calculations, and between 23 and 400 W/m/K using first-principles anharmonic scattering calculations. Besides the dispersion of the values, the physical mechanisms governing the heat flux in those materials are not fully explained, particularly how the properties change with the material composition, thickness and scattering sources. Several works have gone in this direction for bulk TMDs [22,24] providing precious insight, but either using $T = 0$ K interatomic force constants, or for a limited set of TMDs.

Here, we carry out a detailed investigation to unravel the microscopic mechanisms governing heat dissipation in different TMDs, and conduct a comparative study of the thermal properties of the most common TMDs in both their bulk and monolayer structures, using a rigorous method based on first-principles calculations, thermally renormalized phonons and the iterative solution of the Boltzmann transport equation (BTE). The structure of this paper is as follows: In Sec. II we present the methods employed and the calculation details, while the results Sec. III is devoted to present the main findings of this work. We present first the comparison between monolayer and bulk TMDs, focusing on the phonon band structures and on the thermal conductivity. Then, we study the differences between monolayers with different chemical compositions, presenting a microscopic analysis of the

parameters that play a role in the thermal conductivity. We analyze the effect of the atomic species on both phonon bands and κ_l by studying artificial TMDs with modified mass of the compounds, while keeping the crystal interatomic force constants fixed. Finally, we show how the thermal properties depend on the dimensionality of the crystal bonding: we compare a 3D bonded bulk crystal, silicon, to a silicon monolayer, silicene and 2D-bonded bulk TMDs with monolayer TMDs. Section IV draws the main conclusions of our work. In Appendix we report a detailed analysis of the scattering rates occurring in our materials.

II. METHODS

In our calculations we consider a hexagonal unit cell and the stable 2H stacking for the bulk. The monolayer calculations are performed cutting out and relaxing a single layer from the bulk structure. The approach used to compute the thermal properties is based on density functional theory (DFT) [25,26] as implemented in the SIESTA program [27,28], combined with the temperature-dependent effective potentials method (TDEP) [29–31] for anharmonic lattice dynamics and thermal transport. The *ab initio* calculations are used as a driver for computing the atomic forces needed as input for the calculation of the thermal properties. The atomic positions and lattice constants are optimized using a conjugate gradient minimization scheme. The reference structures, from material project database [32], are relaxed until the maximum forces on atoms were smaller than 10^{-5} eV/Å. Our DFT calculations are performed using the GGA-PBE [33] functional including van der Waals interactions through the LMKLL parametrization [34]. A cutoff energy of 1000 Ry is used for the real space integrals, and the Brillouin zone sampling is performed with a mesh of $20 \times 20 \times 20$ k points in the bulk systems and $20 \times 20 \times 1$ for the monolayers. All the pseudopotentials are taken from the PSEUDODOJO library [35] in the scalar relativistic norm conserving form [36]. Phonons and anharmonic terms are computed using the DFT forces obtained with SIESTA, in supercells of sizes $10 \times 10 \times 2$ for bulk and $10 \times 10 \times 1$ for monolayer systems.

In order to obtain the thermal properties, we employ the TDEP method, which has been used successfully in many systems of different bonding and dimensionality [37–40]. For the case of MoSe₂ we have previously utilized TDEP combined with SIESTA to calculate the thermal conductivity in a broad range of thicknesses, from the bulk down to the monolayer limit, in excellent agreement with experimental results [41].

We displace the atoms using thermally occupied phonon displacements following a Bose-Einstein distribution at 300 K [30,31,42]. Initial force constants are built from a model quartic potential fit to the Debye temperature taken from the literature [16,17,43]. With those generated supercells, statistically distributed to sample a canonical ensemble, we extract second- and third-order interatomic force constants (IFCs). The IFCs are obtained by fitting the potential energy surface at finite temperature in order to get the best possible effective Hamiltonian. These IFCs are then used to generate new thermalized and stochastic configurations and to extract a new set of IFCs for the system, iterating until self-consistency is reached. In our calculations we use a number of canonical

configurations $N_{\text{conf}} = 2^p$, where p is the iteration number. We need seven iterations to converge the IFCs for the materials studied, leading to a total of 128 configurations. We computed the IFCs using a radial cutoffs of 8 Å and 5 Å for second- and third-order IFCs, respectively. We have checked that TDEP does not generate configurations with unphysical bond lengths in our TMDs, as can happen for graphene [44], and therefore its application in these systems is sound.

In order to converge the force constants we compute the phonon dispersions and the thermal conductivity at each iteration step. We consider that the calculation is converged when the maximum relative difference in the phonon frequencies and the lattice thermal conductivity in the in-plane direction between consecutive iterations is less than 1%. For the range of the IFC, we have checked the IFCs' norm, in order to verify how small the interactions on the last shell were. With the final IFCs, κ_l is obtained by solving the linearized BTE iteratively. The first step of the iteration is the relaxation time approximation (RTA), where mean-field single-phonon lifetimes are used. In order to extract the lattice thermal conductivity, we perform the calculations for different q -point grids, up to $24 \times 24 \times 24$ for bulk crystals and $128 \times 128 \times 1$ in the monolayers, and extrapolate to an infinite grid of q points using a linear fit of $1/\kappa_l$ versus $1/N_{qx}$ where x indicates the in-plane direction, as reported in the literature [45]. Here we recall the linearized BTE equation valid for small perturbations out of equilibrium, within the RTA, in order to understand which physical parameters play a dominant role for our purposes:

$$\kappa_{\alpha\beta} = \frac{1}{V} \sum_{\lambda} C_{\lambda} v_{g\alpha\lambda} v_{g\beta\lambda} \tau_{\lambda}, \quad (1)$$

where λ indicates the phonon mode, V is the volume of the simulation cell for the material studied—in our case the volume used to perform the DFT calculations— C_{λ} is the volumetric specific heat capacity of the mode, v_{λ} is the mode group velocity, τ_{λ} is the mode-specific phonon lifetime, and α and β indicate the directions where the temperature gradient is applied and where the heat current is measured, respectively [4]. The first two quantities (C_{λ} and $v_{g\lambda}$) depend only on the second derivatives of the energy with respect the atomic displacements, while τ_{λ} includes all the anharmonic effects, and depends on the higher orders of the energy vs displacement derivatives. In the TDEP method the second-order IFCs are renormalized to infinite order, which minimizes the explicit higher-order terms, and optimizes for the applicability of perturbation theory. Within TDEP the temperature-dependent fit yields the best harmonic model, which includes the average (over the configurations chosen) contributions of all higher order terms. This implies that the fit of the higher-order terms (beyond the harmonic ones) produces the smallest values, as they are only the difference between the full anharmonic terms and their average value contributing to the harmonic term. The fact that the anharmonic terms are small significantly increases the range of applicability of perturbation theory starting from the effective harmonic one. To quantify the accuracy of our method to describe the thermal conductivity, we analyze the effect of the different phonon scattering processes, including isotope and four-phonon scattering, showing

the results in Appendix. We demonstrate that the contribution due to four-phonon scattering is small (few percent). For that reason, we limit the anharmonic terms in the fit to the third derivatives, ignoring explicit scattering coming from higher orders. For MoS₂, the isotope scattering decreases the thermal conductivity by 25% at room temperature in the bulk case, and 18% in the monolayer. Similar changes are found for the other TMDs; more specifically, for the bulk (monolayer) we find a decrease of 38% (17%) for WS₂, 15% (8%) for MoSe₂, and 15% (6%) for WSe₂.

The computed values refer to the cell used in the simulation. In the case of the monolayers we consider a c parameter that includes 17 Å of vacuum, which is sufficient to prevent any periodic interactions along the stacking direction. Some of the studies presented in the literature include a different choice of the monolayer thickness used in the calculation of the thermal conductivity, and the correct definition of the effective thermal thickness is still under debate. A recent work proposed a thickness-free definition of thermal conductivity for two-dimensional materials, called sheet thermal conductivity [46]. However, the conversion of the literature values to this new definition is not straightforward: in many works it is not clear what thickness was used, and moreover, the sheet conductivity makes the comparison with experiments more complicated. Here, we consider the thickness (for one monolayer plus vacuum) as the value that gives us the best agreement with the experimental results [41] across many thicknesses, and note that this particular choice does not qualitatively affect the conclusions on the microscopic mechanisms in our comparative study.

III. RESULTS

In this section, we analyze the thermal properties of the four most commonly used TMDs in their monolayer and bulk forms: MoS₂, WS₂, MoSe₂, and WSe₂. First, we compare the monolayers with their bulk counterparts, and then focus on the differences between the various monolayers (Sec. III A). We start by analyzing the phonon dispersion and density of states (phonon DoS) (Sec. III A 1), then we study the in-plane thermal conductivity and compare monolayer values with the theoretical literature, in which κ_l is still under debate, and with the bulk results (Sec. III A 2).

To understand the microscopic properties that determine the thermal conductivity in these materials, we carry out an analysis of (i) the spectral conductivities, to evaluate the frequency range of phonon modes that contribute most to the thermal transport; (ii) the group velocity, heat capacity and phonon lifetimes to understand the differences between the four compounds (Sec. III A 3), and (iii) the effect of the atomic species on the thermal properties (Sec. III B). Lastly, we present the comparison with silicon and silicene, to understand the effect of the bonding type and dimensionality on the thermal properties (Sec. III C).

A. TMDs: bulk vs monolayer

We start with a detailed analysis of the phonon band structures and phonon density of states for a better comprehension of the nature of the underlying phonon modes, and to explain

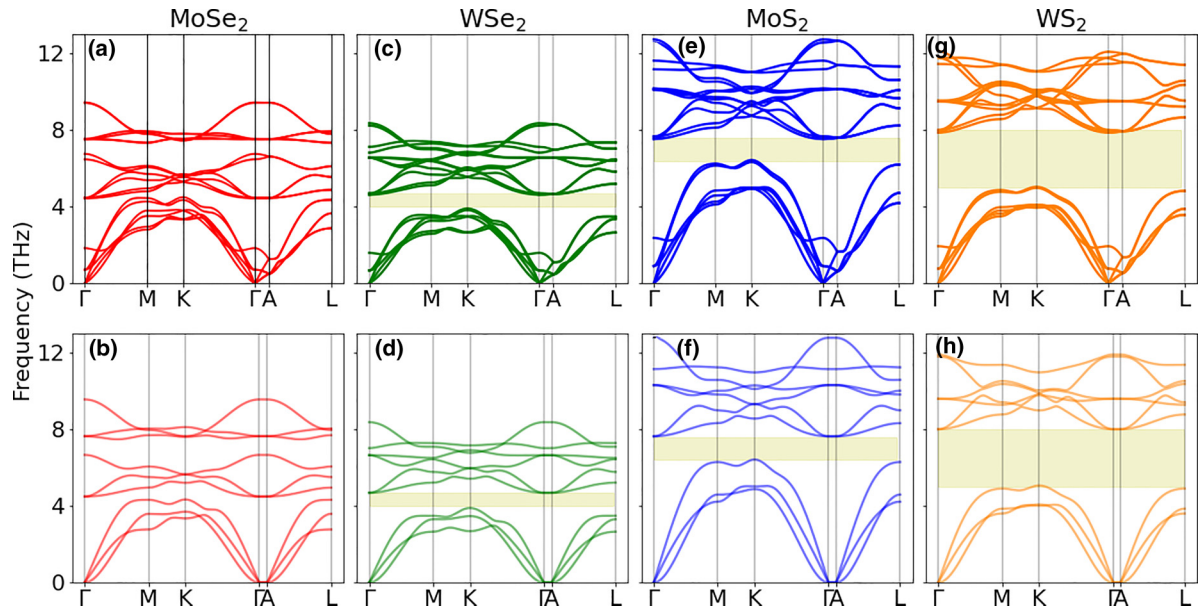


FIG. 1. Phonon band structures of bulk (top) and monolayers (bottom) TMDs. Yellow shaded regions show the band gap between the optical and acoustic (or acousti-like interlayer) modes. For the monolayers, to facilitate the comparison with bulk, we also show directions of the Brillouin zone perpendicular to the layer (Γ -A), although there is no phonon dispersion in that direction.

how the thickness of these materials affects their vibrational properties (Fig. 1 and Fig. 2). Then, we compare our in-plane thermal conductivity with literature results for the monolayer and bulk TMDs (Tables I and II). In addition, we report in Fig. 3 intermediate microscopic quantities that enter in the thermal conductivity, to show the influence of each independently.

1. Phonon dispersions of TMDs

The phonon dispersion relations shown in Fig. 1 are similar for the four TMDs under study, with a change in the frequency range due to the different species of atoms involved; the lighter the chalcogen, the higher the frequency range of the phonons. The acoustic modes have a markedly mixed character for the selenides (where the mass of the metal and the chalcogen are closer), but their character is dominated by

the metal atom for the sulfides. These arguments also explain the width of the acoustic manifold, which decreases when going from Mo to W, and increases when changing Se by S. For the optical modes, the phonon character is necessarily complementary: the weight shifts towards the chalcogen atom as the mass difference increases. Note that some optical modes have pure chalcogen nature imposed by symmetry (see, e.g., Ref. [47]). The two sulfides exhibit a substantial phonon band gap between the acoustic and optical manifolds, which is smaller in WSe₂ and absent in MoSe₂. This feature was correlated with the thermal conductivity by Broido, Lindsay and coworkers: a larger phonon band gap causes a higher thermal conductivity due to the limitation of anharmonic processes, particularly those involving two acoustic phonons and an optical phonon (*aa* scattering) [48,49]. In the case of MoSe₂, where the masses of the atoms are closest, the phonon DoS [Figs. 2(a)–2(b)] shows the strongest mixing of atomic

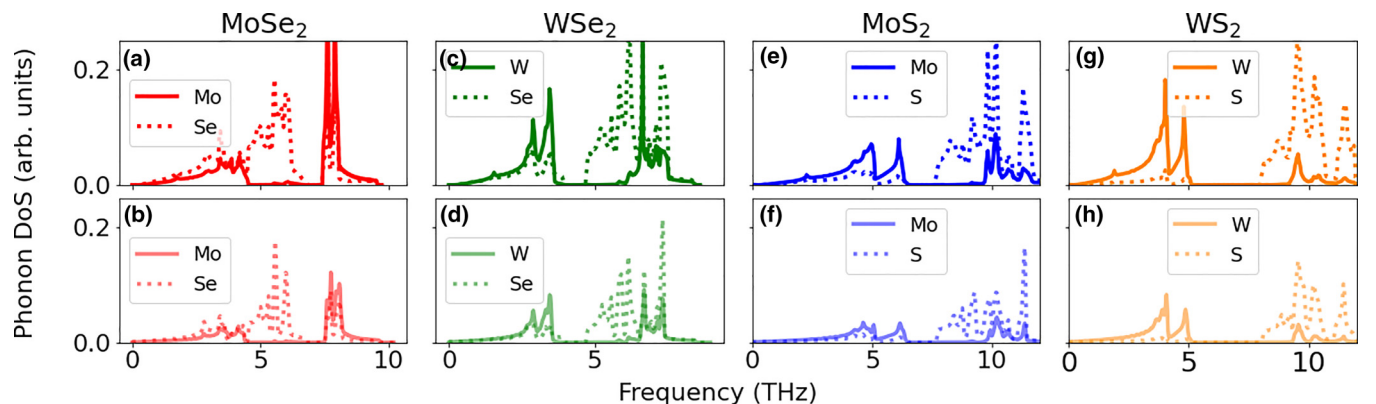


FIG. 2. Phonon DoS of bulk (top) and monolayers (bottom) TMDs. Dashed and solid lines represent the DoS projected on the chalcogen and on the metal atoms, respectively.

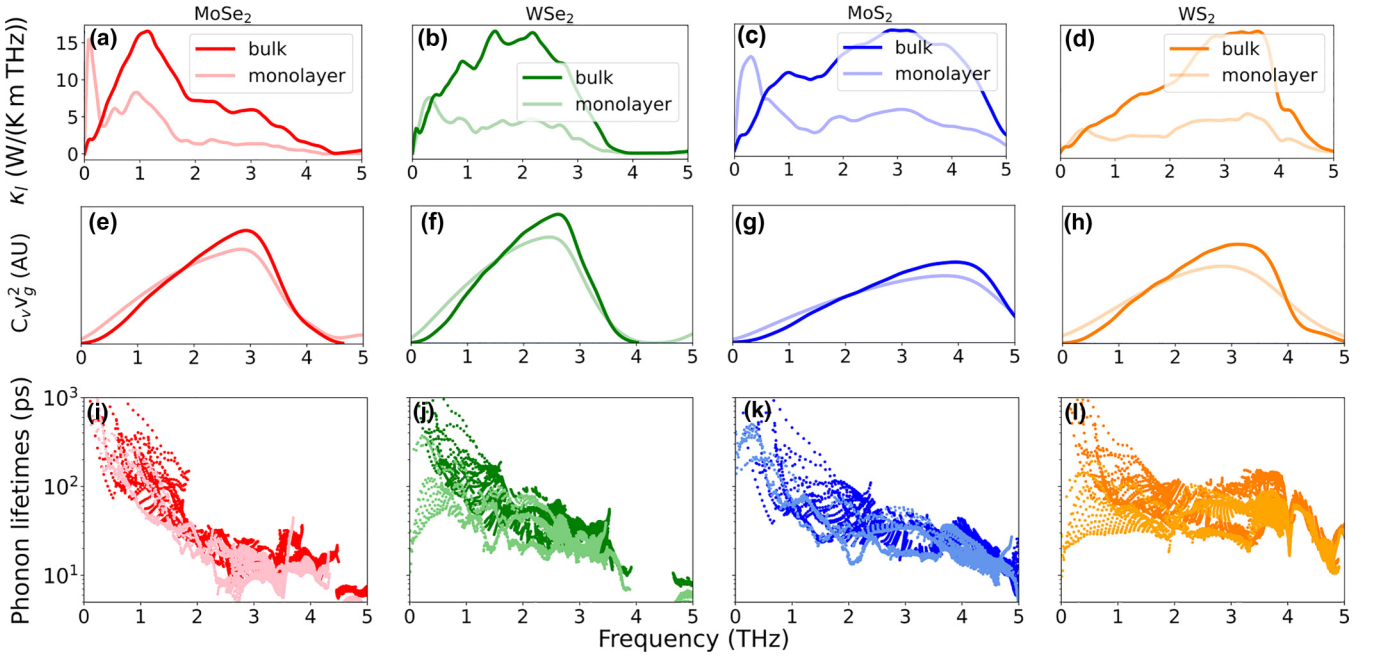


FIG. 3. Thermal properties of TMDs in the bulk (darker colors) and monolayer structures (lighter colors). (a)–(d) show the spectral thermal conductivity, i.e., the thermal conductivity resolved in frequency. The total area under the curve represents the effective thermal conductivity. (e)–(h) are the product of heat capacity and group velocity square $C_v v_g^2$. (i)–(l) show the phonon lifetimes.

character at low frequencies. In this case there is no gap between the two manifolds [Figs. 1(a) and 1(b)] and we obtain the lowest values for the thermal conductivity, as we will show in Sec. III A 2.

2. Thermal conductivity for monolayer and bulk TMDs

Heat transport in TMDs is naturally dominated by the three acoustic phonon branches: the longitudinal acoustic (LA), transverse acoustic (TA), and flexural acoustic (ZA) modes. The LA mode involves compression waves with atomic displacements along the wave propagation direction. The TA mode corresponds to shear waves with in-plane displacements perpendicular to the propagation direction. Lastly, the ZA mode involves out-of-plane atomic displacements. While the LA and TA branches have approximately linear dispersion at the center of the Brillouin zone, the monolayer ZA mode shows a quadratic dispersion as expected for 2D structures [50,51]. In the case of bulk crystals a large contribution comes from the low-lying (acousticlike) optical phonon modes, which have similar group velocities and only slightly higher frequencies than pure acoustic modes.

We summarize our calculated values of the in-plane thermal conductivity for monolayer TMDs in Table I, together with predicted values reported in the literature obtained using nonequilibrium molecular dynamics (NEMD) [8], the *ab initio* Peierls-Boltzmann equation, the semiempirical Slack equation [9], the Green Kubo (GK) [52,53] formalism, and the nonequilibrium Green's function (NEGF) [10] method. The variation in the values reported in the literature can have different origins, some of which can be: (i) the specific force field and approximations made in the molecular dynamics studies; (ii) the size of the supercell used for the simulations: NEMD

studies implement an explicit gradient, which is often unrealistically high and may be beyond the linear Fourier regime; (iii) the monolayer thickness assumed in the calculation of a volume (the thermal conductivity being inversely proportional to its value); and (iv) the scattering sources taken into account (see below). Our results align with the lower values of conductivities reported in the literature. The two selenides have similar thermal conductivities, while those of MoS₂ and WS₂ are 1.5× and 2× larger, respectively. This trend is in line with previous studies reporting the in-plane thermal conductivity for the four TMDs, obtained experimentally by time-domain thermoreflectance [54], spatiotemporal measurements of phonon diffusion [55], and obtained theoretically using DFT and the Boltzmann transport equation [19,22].

In Table II we report the in-plane thermal conductivity for the bulk TMDs calculated in this work and compared with the literature. Our results match with previous works using similar methods [60,61], while the predicted value of κ_l of MoS₂ obtained using NEMD [59] is considerably lower, 75%, than our results, and found to be constant with the number of layers, suggesting a possible underestimation of the interlayer interactions due to the choice of the empirical potential. Overall, the monolayer values are two to three times lower than the bulk, which reflects confinement effects. We will now examine which phonons are affected by interlayer interactions.

3. Microscopic analysis of the thermal conductivity in TMDs

To pinpoint which phonons dominate thermal transport, we plot the spectral thermal conductivity [Figs. 3(a)–3(d)], which represents the integrand of κ_l in the frequency domain. We plot the range of modes below 5 THz, and note that the

TABLE I. Literature values for theoretical predictions of κ_l in monolayer TMDs at room temperature, indicating in each case the method used in the calculations. Nonequilibrium Green's function (NEGF) [10], Green Kubo (GK) [52,53], nonequilibrium molecular dynamics (NEMD) [8], DFT results either in the Peierls-Boltzmann (BTE) method [4] or the semiempirical Slack approach [9].

TMD	Method	in-plane κ_l (W/m/K)	Reference
MoSe ₂	DFT + Slack	17.6	[16]
MoSe ₂	NEMD	24.8	[12]
MoSe ₂	NEMD	29.05	[56]
MoSe ₂	NEMD	~40	[23]
MoSe ₂	DFT + BTE	54	[19]
MoSe ₂	DFT + BTE	51.5, 70.3	[24]
MoSe ₂	DFT + GK	39	[24]
MoSe ₂	DFT + BTE	20.6	This work
WSe ₂	NEMD	39.94	[56]
WSe ₂	DFT + BTE	3.93	[57]
WSe ₂	DFT + BTE	51	[58]
WSe ₂	DFT + BTE	53	[19]
WSe ₂	DFT + BTE	58.7, 55.1	[24]
WSe ₂	DFT + GK	42	[24]
WSe ₂	DFT + BTE	21.8	This work
MoS ₂	NEMD	1.35	[11]
MoS ₂	NEMD	32.9	[12]
MoS ₂	NEMD	193–531	[13]
MoS ₂	NEMD	33–54	[14]
MoS ₂	NEMD	19.76	[59]
MoS ₂	NEMD	89.43	[56]
MoS ₂	NEMD	~90	[23]
MoS ₂	NEGF	23	[15]
MoS ₂	DFT + Slack	33.6	[16]
MoS ₂	DFT + BTE	34.5	[17]
MoS ₂	DFT + BTE	83	[18]
MoS ₂	DFT + BTE	103	[19]
MoS ₂	DFT + BTE	131	[20]
MoS ₂	DFT + BTE	~400	[21]
MoS ₂	DFT + BTE	32.4	This work
WS ₂	NEMD	91.66	[56]
WS ₂	DFT + Slack	31.8	[16]
WS ₂	DFT + BTE	142	[19]
WS ₂	DFT + BTE	42.4	This work

monolayer spectral conductivity is significantly smaller with respect to bulk. Interestingly, in the very low frequency range (below 0.5 THz), we see a contribution in the monolayer MoS₂ and MoSe₂ spectra that is not present in the bulk, and that partially compensates the smaller contribution from the rest of the frequency range [Figs. 3(a), 3(b)]. In Figs. 3(e)–3(h) we show the harmonic contribution ($\int C_v v_g^2$) of the phonons to the total thermal conductivity [see Eq. (1)] in monolayer and bulk TMDs. The difference in the thermal conductivity cannot be explained by the harmonic term: only minor changes appear between the bulk and the monolayer, resulting from (i) the quadratic flexural mode present only in the monolayer and in (ii) the acousticlike optical modes in the bulk TMDs. The latter are the combination of acoustic modes of the monolayer constituents, but with different phases between consecutive layers. In Figs. 3(i)–3(l) we report the phonon lifetimes as a function of their frequency.

TABLE II. Literature values for theoretical predictions of in-plane κ_l in bulk TMDs, indicating in each case the method used in the calculation.

TMD	Method	in-plane κ_l (W/m/K)	Reference
MoSe ₂	DFT + BTE	55	[60]
MoSe ₂	DFT + BTE	19	[22]
MoSe ₂	DFT + BTE	43.7	This work
WSe ₂	DFT + BTE	50	[60]
WSe ₂	DFT + BTE	42	[22]
WSe ₂	DFT + BTE	52.1	This work
MoS ₂	NEMD	19.76	[59]
MoS ₂	DFT + BTE	98	[61]
MoS ₂	DFT + BTE	81	[22]
MoS ₂	DFT + BTE	76.2	This work
WS ₂	DFT + Slack	31.8	[16]
WS ₂	DFT + BTE	126	[22]
WS ₂	DFT + BTE	134.2	This work

All the materials show decreasing lifetimes as the frequency increases, because more resistive scattering channels become available for higher phonon energies [48]. The peak encountered in the spectral thermal conductivity for monolayers Mo compounds can be explained by large lifetimes at extremely low frequencies below 0.5 THz. The corresponding modes in W TMD monolayers have much smaller lifetimes compared to Mo or the bulk W TMDs, and do not contribute to $\kappa_l(\omega)$. The acoustic mode-resolved lifetimes for the monolayers are shown in Fig. 4, with the corresponding band structures as insets. The majority of the thermal conductivity is explained by the LA phonon mode, associated with larger group velocities, and to the amplitude of the acoustic-optical band gap in the phonon spectrum, which reduces the channels for two phonons to be combined into an optical phonon in the upper manifold. This produces longer phonon lifetimes in the most relevant frequency range for TMDs from 2–4 THz. Both the gaps and lifetimes track the ordering of κ_l : WS₂ > MoS₂ > WSe₂ > MoSe₂. The 2–4 THz frequencies contributing to thermal transport are due to the extended linear dispersion of the acoustic modes (and of the acousticlike, optical modes in the bulk, which have a parallel dispersion).

In the previous literature, some studies predicted infinite phonon lifetimes associated with the ZA mode, due to its quadratic dispersion in q [62]. This artificial feature, derived from the perturbation theory including only three-phonon scattering, is not observed here. Indeed, all our calculations include the natural isotope distribution, which makes the divergence in the lifetimes at low frequency disappear.

The higher thermal conductivity in WS₂ (bulk: 134; monolayer: 42 W/m/K) compared to the other materials is mainly due to the lifetimes of all three acoustic phonon modes. Both in monolayer and bulk WS₂, we see a plateau in the frequency range between 1 and 4 THz, which is unusual comparing to normal materials and simple models where $\tau \sim 1/\omega$, exploits the full peak of the harmonic spectral density.

MoS₂ (bulk: 76; monolayer: 32 W/m/K) is similar, with relatively constant but slightly lower phonon lifetimes from 2–4 THz. The strongest difference is in the ZA mode lifetime, which is two orders of magnitude larger than in WS₂ at very low frequencies.

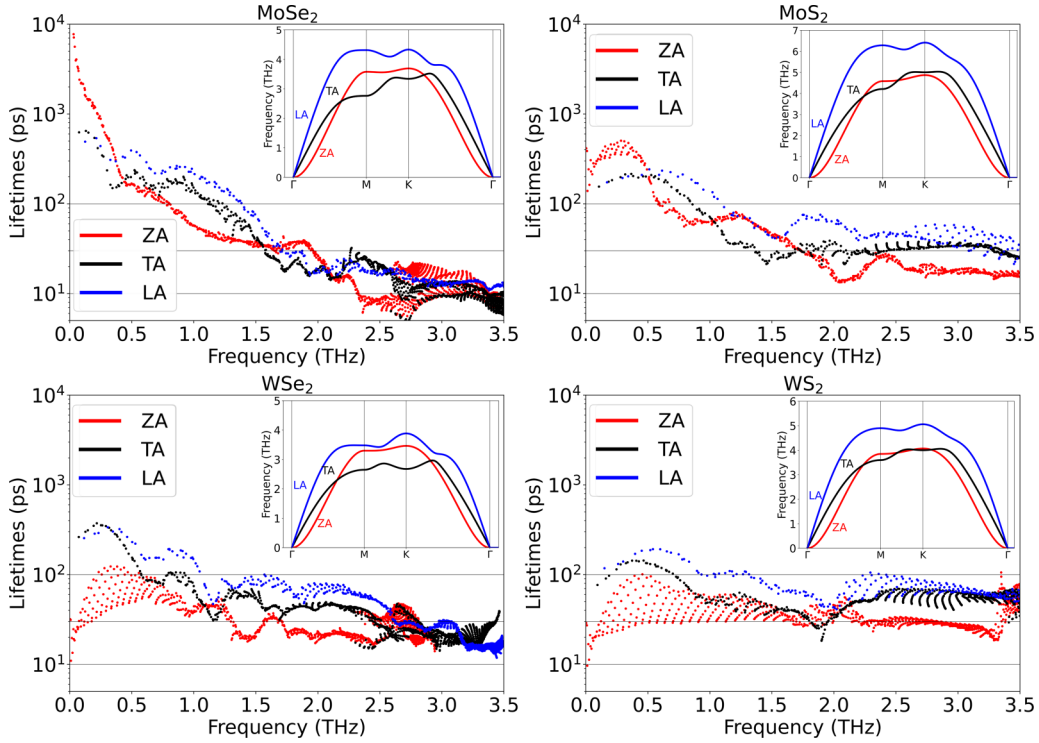


FIG. 4. Phonon lifetimes contributions of the acoustic modes of monolayer TMDs. Insets: acoustic phonon mode dispersions considered in the analysis.

WSe₂ (bulk: 52; monolayer: 22 W/m/K) shows similar lifetimes to WS₂ up to 1.5 THz, but then loses a factor of 2 in ZA and then in LA and TA as well, and has a cutoff before 4 THz resulting from a smaller phonon band gap.

MoSe₂ (bulk: 44; monolayer: 21 W/m/K) presents the sharpest decrease in phonon lifetimes with increasing frequency, in both the monolayer and the bulk case. The shorter lifetimes above 1.5 THz are responsible for the lower thermal conductivity observed in MoSe₂ compared to the other TMDs. The strong acoustic-optical scattering in this material results from the absence of a phonon gap. MoSe₂ presents very long-lived ZA phonons at frequencies lower than 0.2 THz, but their contribution to the overall thermal conductivity is limited by their small velocity, phonon DoS, and hence the C_v .

Despite the fact that the monolayers under study have relatively similar values of the in-plane thermal conductivity, the relative mode contributions to the phonon-phonon scattering are different. In Table III we summarize the percentage contribution of each acoustic mode to the total lattice thermal conductivity. In the W-based TMDs the ZA

TABLE III. Percentage of acoustic contribution to the thermal conductivity κ_l for each mode in monolayer TMDs. The last column reports the percentage of the thermal conductivity that is due to optical modes.

	LA	TA	ZA	Optical modes
MoSe ₂	53.86%	28.75%	16.67%	0.72%
MoS ₂	50.79%	29.51%	18.95%	0.74%
WSe ₂	46.51%	27.32%	25.27%	0.90%
WS ₂	45.01%	28.97%	25.02%	1%

mode has a larger share, close to TA, and the fraction of heat carried by the LA mode is lower. This results from a larger lifetime for the TA modes but a different distribution of the harmonic κ_l factor $C_v v_g^2$.

These results are in agreement with Ref. [58] on WSe₂. In this work, the authors conclude that ZA and TA contributions are comparable because of an enhanced phonon-phonon scattering phase space of the flexural mode, associated with the breaking of the reflection symmetry. This scattering reduces the ZA contribution to the total lattice thermal conductivity [63,64].

In the case of MoSe₂, predicted to be the most anharmonic of our TMDs, the ZA mode contributes only 16.8% of the acoustic thermal conductivity. This reduction is in line with the previous literature [56].

B. Comparison to artificial TMDs with modified mass

To verify whether the thermal conductivity differences among the TMDs can be explained by their relative atomic masses alone, or if there are essential differences coming from details in the chemical bonds through the (harmonic and anharmonic) force constants, we compute the thermal properties of some of the compounds changing their atomic masses but maintaining the IFCs fixed. In particular, we calculated the modified in-plane thermal conductivity κ_l of the most conductive TMD (WS₂) in its monolayer structure, substituting the mass of tungsten by that of molybdenum, indicated with the notation Mo_W, which will increase the phonon frequencies. Comparing the modified in-plane thermal conductivity of these artificial compounds with our results for WS₂ and MoS₂ we can extract relevant information about the origin

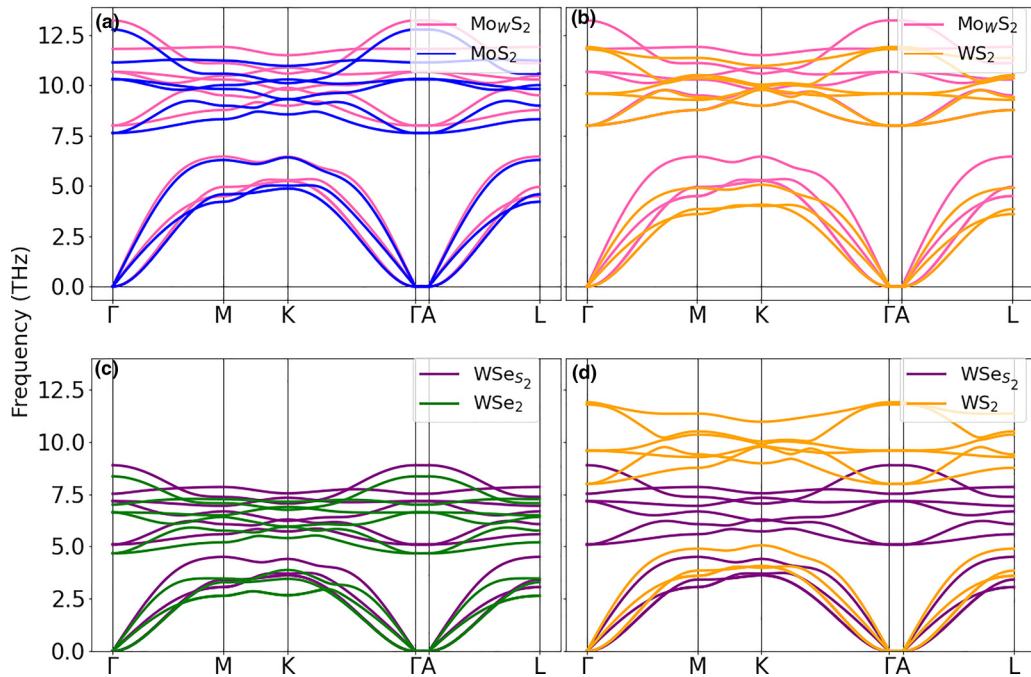


FIG. 5. Phonon band structure of monolayer TMDs with natural and modified masses: (a) and (b) Mo_WS_2 (blue), WS_2 (yellow), and artificial WS_2 with Mo mass in place of W (pink); (c) and (d) WSe_2 (green), WS_2 (yellow), and artificial WS_2 with Se mass instead of S (purple).

of the differences in phonons and thermal properties among the TMDs. Next, we repeat the analysis by changing the sulfur mass to that of selenium, Se_S , which reduces the mass gap. Figure 5 shows the modified phonon band structures according to the mass of the artificial compounds, compared to the four reference TMDs. The left panels, Figs. 5(a) and 5(c) demonstrate the effect of the IFCs, while the right panels, Figs. 5(b) and 5(d), show the effect of the mass change with respect to WS_2 . As expected the harmonic part of the κ_l integral indeed depends strongly on the relative mass difference between the two species involved. In the first case [Fig. 5(a)] the WS_2 IFCs have a small effect, pushing the optical phonon frequencies slightly higher. In Fig. 5(b) we observe more energetic phonons in the acoustic range due to the lighter metal, but also a change of 10% in the optical phonon energy. The acoustic optical gap decreases on net with respect to WS_2 . When substituting the S with Se atoms [Fig. 5(c)], there are changes in both the acoustic and optical manifolds, and the phonon band gap decreases with respect to the WSe_2 . Finally in Fig. 5(d) we see the largest effect, coming from a chalcogen mass change in WS_2 .

The changes in acoustic and optical phonons could be expected to remove/create scattering channels in the modified compound, leading to an increase/reduction of the thermal conductivity. This can be qualitatively verified through the spectral thermal conductivity and lifetimes in Fig. 6. By looking in more detail at the anharmonic part, particularly at the phonon lifetimes, we can see that the mass substitution has indirect effects in the trend of the thermal conductivity. For the Mo_W substitution the higher-frequency lifetimes decrease, and the low-frequency Mo peak does not appear; it is intrinsic in the Mo IFC. For the Se_S substitution there is also a high-frequency suppression of the lifetimes, and the $\kappa_l(\omega)$ becomes

almost identical to WSe_2 ; the chalcogen difference is mainly a mass effect except a few low-frequency phonons in WSe_2 , which do not affect $\kappa_l(\omega)$. Combining the IFCs of the original compounds and the masses of the modified structure, the in-plane thermal conductivity of WS_2 (42.4 W/m/K) decreases, whether with the Mo or Se substitutions, to values of 19.4 and 32.0 W/m/K, respectively.

C. Comparison with silicon

So far, we have focused our attention on the differences between the TMDs. In this section we also consider the

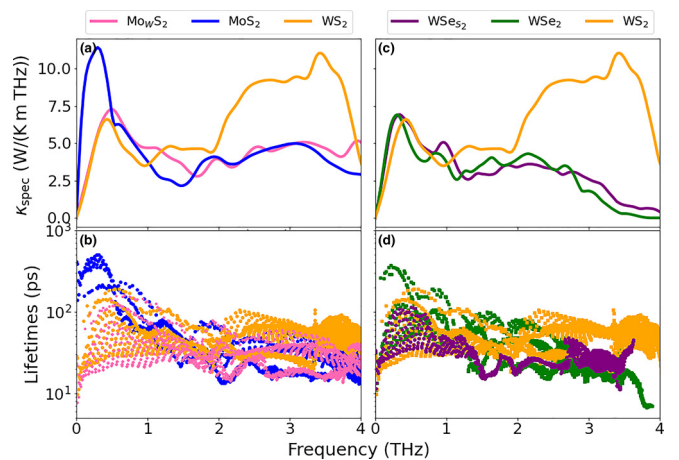


FIG. 6. Lattice spectral thermal conductivity (top panels) and phonon lifetimes (bottom) for modified WS_2 , compared to those of the MoS_2 , WS_2 , and WSe_2 compounds. Left panels show the results for artificial TMDs with replacement of the W mass by that of Mo, and right panels using Se mass in place of S.

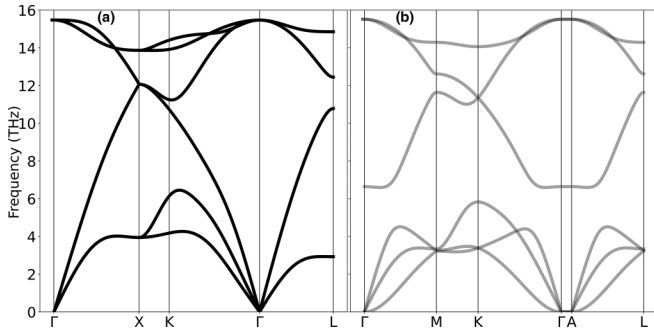


FIG. 7. Phonon dispersion relations of (a) bulk silicon and (b) monolayer silicene.

effect of the type of interlayer bonding (covalent vs van der Waals) on the thermal conductivity. We consider the thermal properties of monolayer silicon (silicene) and compare it with bulk silicon. To model silicene we select a honeycomb lattice with low buckling obtained from a Si(111) surface. Previous *ab initio* studies have shown this to be the most stable structure resulting from a pseudo-Jahn–Teller effect, which is present only in the monolayer structure [65–69].

Figure 7 displays the phonon dispersion relations of monolayer and bulk silicon, which align with prior research [48,70]. The most noticeable difference between bulk and monolayer is in the acoustic manifold.

The bulk silicon phonon structure is continuous between its acoustic and optical manifolds and shows a large group velocity for the LA branch. Whereas TMDs display little change in phonon structure due to thickness, in the case of silicene a gap appears that changes the interactions between acoustic and optical phonons, and the group velocity of longitudinal and especially ZA acoustic phonons is reduced, which limits the thermal transport.

From the spectral thermal conductivity [Fig. 8(a)] we can see a broad drop in κ_l contributions across the spectrum from the bulk to the silicene layer. The first effect arises in the harmonic term [Fig. 8(b)] at frequencies larger than 3 THz, where the strong reduction of group velocities explains a part of the drop in the thermal conductivity between silicon and silicene. This is a true 2D/3D effect, and is not observed in the TMDs: in the midranged acoustic frequencies, the silicene LA phonon group velocity goes to zero, giving a much lower contribution to the thermal conductivity. However, most heat transport in bulk silicon comes from phonons with relative low energies, in the range between 1 THz and 3 THz, where the harmonic term does not change as much, and can even be larger in silicene than bulk silicon. In Fig. 8(c) we present the phonon lifetimes: there is a change of two orders of magnitude in phonon lifetimes between the bulk and the monolayer, particularly in the acoustic phonon bands, where bulk silicon shows phonon lifetimes of 1 ns against a maximum in silicene of dozens of ps. The long-lived low- q phonons lead to the large value observed in bulk silicon, and the strong difference with its monolayer counterpart. The cumulative thermal conductivity with respect to mean-free path (Fig. 9) confirms this: the phonons in bulk silicon give significant contributions for mean-free paths up to 30 μm . Phonons with MFP up to

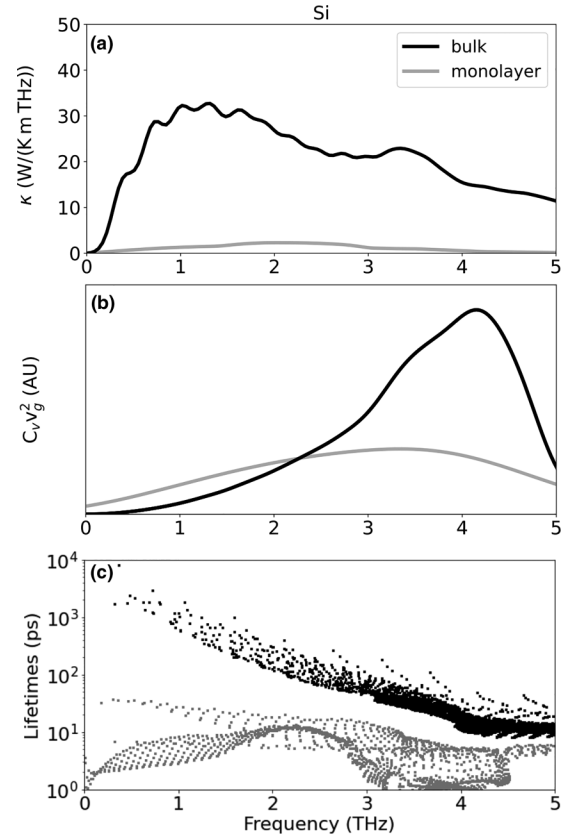


FIG. 8. Bulk silicon (black) and monolayer silicene (gray) properties: (a) Spectral thermal conductivity, (b) harmonic contribution to the thermal conductivity, and (c) phonon lifetimes.

100 nm comprise the whole thermal conductivity in silicene, but contribute only for 25% of the bulk κ_l .

The origin of this behavior is naturally the different bonding type in the two compounds. In the case of the layered vdW structures, the forces do not change strongly when passing from a monolayer to a bulk structure, since the chemical nature of the compound remains the same and interlayer interactions are always weak. The lack of covalent bonds in the silicene structure in the out-of-plane direction, together with the strong anisotropy of the monolayer compared to the

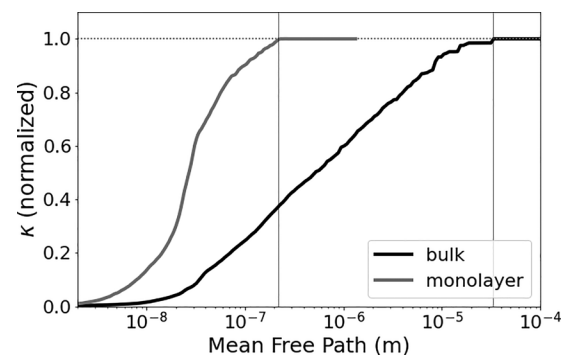


FIG. 9. Thermal conductivity as a function of the total phonon mean-free path for bulk silicon (black) and silicene monolayer (gray). The vertical lines represents the phonon mean-free path at which the whole conductivity is taken into account.

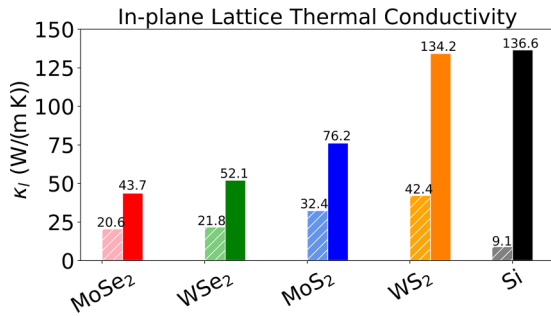


FIG. 10. Thermal conductivity vs thickness: the length of the histogram represents the in-plane thermal conductivity expressed in units of W/m/K for the compounds studied using SIESTA DFT and BTE as implemented in TDEP. The shaded bars represent the monolayer structure, the uniformly coloured bars represent the bulk values. In the case of the monolayers we consider a c parameter that includes 17 Å of vacuum. If, instead we would use the thickness of a single layer of compound, obtained as half of the c lattice parameter in the bulk structure, the thermal conductivity of monolayer TMDs would be, respectively: MoSe₂ 53.87 W/m/K, WSe₂ 56.33 W/m/K, MoS₂ 89.17 W/m/K, WS₂ 116.44 W/m/K.

cubic 3D crystal, change its properties drastically. Indeed, according to the Slack’s criteria [9], one of the rules of thumb to have high thermal conductivity in nonmetallic structures is the presence of strong interatomic bonds. These bonds are much less numerous in 2D silicene than in bulk Si, which causes a strong decrease in its heat conduction efficiency. While flexural phonons can also contribute to heat transport in 2D materials, they are not sufficient to compensate for the loss of effectiveness of these types of bonds. Another important difference is the presence of long MFP phonons at midfrequency, known in the literature for bulk silicon [45], which are absent in silicene.

In Fig. 10, we present a comprehensive summary of our calculated in-plane lattice thermal conductivities, and compare the bulk values with the monolayer cases, including for silicon. In the TMDs, we observe a reduction by a factor 2–3 in thermal conductivity when passing from the bulk to the monolayer. On the contrary, due to the difference in the structure and nature of the bonds, 2D silicene presents a reduction by a factor 15 with respect to the bulk silicon, as explained by the analysis above (Sec. III C).

IV. CONCLUSIONS

In summary we have calculated the thermal conductivity and related physical quantities for four different 2H TMDs in their bulk and monolayer forms, using a DFT-BTE approach beyond the relaxation time approximation. We have analyzed the contribution of different phonon modes as a function of frequency and the accessible phase space where phonon-phonon interactions take place. This allows us to identify the parameters responsible for the different heat transport behaviors we observe in these compounds.

The order of the bulk and monolayer TMD κ_l (WS₂ > MoS₂ > WSe₂ > MoSe₂) can be explained by the combination of several factors. The harmonic phonons are quite

similar between the four materials, as is the harmonic spectral contribution to κ_l : $C_v v_g^2(\omega)$. The intermediate frequencies 2–4 THz are important as C_v increases and v_g is maintained for acoustic and acousticlike low optical modes in 2D materials. Lifetimes in this range are determined mostly by the size of the phonon band gaps. A plateau in midfrequency lifetimes and a wider frequency range for WS₂ (and MoS₂) explains its larger thermal conductivity.

The monolayer and bulk TMD κ_l show very little difference in harmonic terms, but some systematic decrease of the lifetimes across the board. The dramatic drop of the low-frequency ZA mode lifetimes has few consequences on κ_l in W-based compounds, while some κ_l is recaptured in the Mo compounds with a low-frequency peak in $\kappa_l(\omega)$ below 0.5 THz. Mass substitution for constant interatomic force constants allows to dissect the effects at low and high frequency: the low-frequency Mo peak is due to the IFC and not to the mass or frequency; the midfrequency dominance of WS₂ on the other hand is linked to frequencies and the mass ratio of W/S, rather than the intrinsic IFC.

While in the case of TMDs, the harmonic term does not change significantly with thickness, it has a remarkable impact on the thermal conductivity of bulk and monolayer silicene, where we observed a decrease of a factor ~ 15 of the in-plane thermal conductivity from the bulk silicon to silicene. This results both from harmonic (reduction of group velocities) and anharmonic effects (band interference scattering). There are almost three orders of magnitude difference between phonon lifetimes of silicene and bulk silicon for frequencies lower than 3 THz, where the majority of the thermal conductivity is taken into account. The interlayer bonding (covalent vs vdW) in the structure is a key factor in determining heat transport.

The findings presented in this work should be generalizable to other TMDs, and to other 2D materials as well, although we observe significant differences already between these four closely related materials. The examination of the phonon dispersions and along with the insight found here might allow a first estimate of the potential for thermal conductivity and related quantities. Moreover, the simple and effective methodology introduced in our study provides a practical means to analyze the thermal properties of TMDs and comparing them with other materials.

ACKNOWLEDGMENTS

We acknowledge Dr. Alois Castellano for providing the 4phi implementation in TDEP useful for computing the four phonons scattering contributions. R.F. and P.O. acknowledge support by the EU H2020-NMBP-TO-IND-2018 project “INTERSECT” (Grant No. 814487) and Grant No. PID2022-139776NB-C62 funded by Spanish MCIN/AEI/10.13039/501100011033 and by ERDF A way of making Europe. R.F. and K.-J.T. acknowledge financial support by the Spanish State Research Agency under Contract No. PID2019-111673GB-I00/AEI/10.13039/501100011033 and the European Union’s Horizon 2020 Research and Innovation Program under Grant Agreement No. 804349 (ERC StG CUHL). M.-J.V. acknowledges funding from ARC project DREAMS (G.A. 21/25-11) funding by the Federation

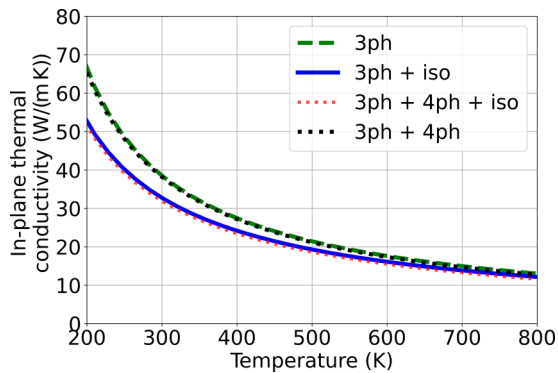


FIG. 11. Thermal conductivity of monolayer MoS₂ as a function of temperature. The comparison takes into account the in-plane κ_l calculated in the main section above (blue line), then without the contribution of isotope disorder scattering (green dashed line) and then including the four-phonon processes that have been proven to play a role in monolayer graphene, including isotope scattering (red dotted line) and without it (black dotted line).

Wallonie Bruxelles and ULiege, Belgium. Z.Z. acknowledges financial support by the Netherlands Sector Plan program 2019-2023 and the research program “Materials for the Quantum Age” (QuMat, registration number 024.005.006), part of the Gravitation program of the Dutch Ministry of Education, Culture and Science (OCW). We acknowledge a PRACE award granting access to MareNostrum4 at Barcelona Supercomputing Center (BSC), Spain and Discoverer in SofiaTech, Bulgaria (OptoSpin Project Id. 2020225411). The ICN2 is supported by the Severo Ochoa Centres of Excellence programme, Grant No. CEX2021-001214-S, funded by MCIN/AEI/10.13039.501100011033

APPENDIX: SCATTERING CONTRIBUTIONS

In this Appendix we will analyze the contribution of different scattering mechanisms present in the 2D crystals.

1. Scattering beyond intrinsic three phonon

An important factor to consider when studying the phonon thermal transport is the relative contribution of the different scattering mechanisms that determine the total thermal conductivity. The analysis is performed on monolayer MoS₂ using as input the same (DFT calculated) displaced atomic configuration energies and forces used in the rest of the paper. We use TDEP to calculate the thermal conductivity (i) including not only the three-phonon processes, but also the four-phonon processes; and (ii) examining isotopic mass disorder following the natural distribution of isotopic masses. Both mechanisms add scattering and therefore thermal resistance. The three cases are compared in Fig. 11. The first contribution (four-phonon processes) is often neglected due to the difficulty in its calculation, with an extremely high computational cost compared to the three-phonon scattering because of the increased phase space for four-phonon (three independent wave vector) events conserving momentum and energy [71]. For bulk crystals it has been shown that these contributions can be important, especially at high temperatures,

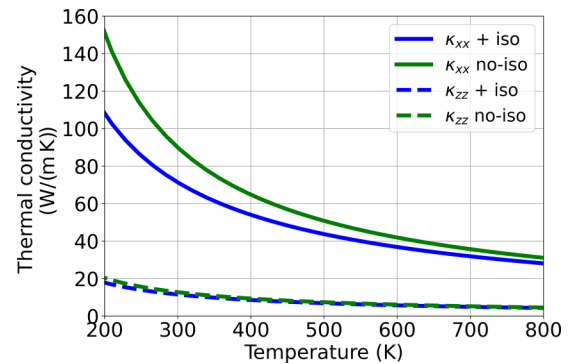


FIG. 12. Lattice thermal conductivity of bulk MoS₂ as a function of temperature between 200 K and 800 K. We show the results for the lattice conductivity κ_l both for the natural isotope distribution (labeled iso) and the isotopically pure case (labeled no-iso), respectively, in blue and green. With solid lines we report the in-plane thermal conductivity and with dashed lines the out-of-plane contribution, with good agreement with previous literature [73,75].

reaching contributions between 25% and 36% for silicon and germanium [71]. More importantly for us, recent studies have shown a large effect in single-layer graphene: the in-plane mirror symmetry forbids processes with odd numbers of out of plane phonons, which reduces the relative ZA branch contribution by 40% [72]. Previous works show contradictory results, with one study finding that four-phonon processes only decrease the thermal conductivity by about 10% [73], and another predicting a decrease of almost a factor of five [74]. We do not observe as strong an effect in monolayer MoS₂ where it yields a contribution to the thermal conductivity of less than 1% for the temperature range considered. The effect is thus much weaker in TMDs with respect to the planar 2D monolayer graphene. MoS₂ also possesses a horizontal mirror plane, but has additional internal degrees of freedom. We rationalize the small contribution as the result of the additional flexibility of z -polarized modes of the TMD, which allow scattering at the three-phonon level, which is only possible at the four-phonon level in graphene (which starts from a much higher κ_l in the three-phonon case). We reached the same conclusion for the other three monolayer TMDs: the in-plane lattice thermal conductivity decrease by 1% when the fourth-order IFCs are included. It is important to mention that the calculation carried out here is done using a coarser q -point grid than those used for the three-phonon processes, due to memory limitations, and is then extrapolated following the same method we used above.

2. Isotope scattering contribution

Isotope disorder plays a significant role in the bulk crystals as well. In Fig. 12 we show the effect of including isotope disorder for bulk MoS₂, compared to the isotopically pure material. We show values for the typical range of temperatures at which devices can operate, both for the in-plane and out-of-plane thermal conductivity. We observe a reduction due to isotope scattering (mainly for the in-plane conductivity) that becomes more important as the temperature decreases, as

expected: at low T the anharmonic phonon-phonon scattering does not play a significant role, thus the mass disorder in the species involved due to the isotope distribution, has a larger

relative weight. For that reason, in our calculations the isotope scattering with natural isotope distribution is always taken into account.

-
- [1] P. Ajayan, P. Kim, and K. Banerjee, Two-dimensional van der Waals materials, *Phys. Today* **69**(9), 38 (2016).
- [2] A. Chaves, J. Azadani, H. Alsalman, D. Da Costa, R. Frisenda, A. Chaves, S. Song, Y. Kim, D. He, J. Zhou, A. Castellanos-Gomez, F. Peeters, Z. Liu, C. Hinkle, S.-H. Oh, P. Ye, S. Koester, Y. H. Lee, P. Avouris, and T. Low, Bandgap engineering of two-dimensional semiconductor materials, *npj 2D Mater. appl.* **4**, 29 (2020).
- [3] S. A. Han, R. Bhatia, and S.-W. Kim, Synthesis, properties and potential applications of two-dimensional transition metal dichalcogenides, *Nano Convergence* **2**, 17 (2015).
- [4] R. Peierls, *Quantum Theory of Solids*, International Series of Monographs on Physics (Clarendon Press, Oxford, 1955).
- [5] M. Born and K. Huang, *Dynamical Theory of Crystal Lattices*, International Series of Monographs on Physics (Clarendon Press, Oxford, 1988).
- [6] L. Lindsay, A. Katre, A. Cepellotti, and N. Mingo, Perspective on *ab initio* phonon thermal transport, *J. Appl. Phys.* **126**, 050902 (2019).
- [7] A. McGaughey and X. Ruan, *2016 IMECE Tutorials on Phonon Transport Modeling* (2017), <https://nanohub.org/resources/25465>.
- [8] B. D. Todd and P. J. Davis, *Nonequilibrium Molecular Dynamics: Theory, Algorithms and Applications* (Cambridge University Press, Cambridge, 2017).
- [9] G. Slack, Nonmetallic crystals with high thermal conductivity, *J. Phys. Chem. Solids* **34**, 321 (1973).
- [10] K. Y. Camsari, S. Chowdhury, and S. Datta, The nonequilibrium green function (NEGF) method, in *Springer Handbooks* (Springer International Publishing, Berlin, 2022), pp. 1583–1599.
- [11] X. Liu, G. Zhang, Q.-X. Pei, and Y.-W. Zhang, Phonon thermal conductivity of monolayer MoS₂ sheet and nanoribbons, *Appl. Phys. Lett.* **103**, 133113 (2013).
- [12] J. Zhang, Y. Hong, X. Wang, Y. Yue, D. Xie, J. Jiang, Y. Xiong, and P. Li, Phonon thermal properties of transition-metal dichalcogenides MoS₂ and MoSe₂ heterostructure, *J. Phys. Chem. C* **121**, 10336 (2017).
- [13] K. Xu, A. J. Gabourie, A. Hashemi, Z. Fan, N. Wei, A. B. Farimani, H.-P. Komsa, A. V. Krasheninnikov, E. Pop, and T. Ala-Nissila, Thermal transport in MoS₂ from molecular dynamics using different empirical potentials, *Phys. Rev. B* **99**, 054303 (2019).
- [14] X. Wang and A. Tabarraei, Phonon thermal conductivity of monolayer MoS₂, *Appl. Phys. Lett.* **108**, 191905 (2016).
- [15] Y. Cai, J. Lan, G. Zhang, and Y.-W. Zhang, Lattice vibrational modes and phonon thermal conductivity of monolayer MoS₂, *Phys. Rev. B* **89**, 035438 (2014).
- [16] B. Peng, H. Zhang, H. Shao, Y. Xu, X. Zhang, and H. Zhu, Thermal conductivity of monolayer MoS₂, MoSe₂ and WS₂: Interplay of mass effect interatomic bonding and anharmonicity, *RSC Adv.* **6**, 5767 (2016).
- [17] J. Su, Z.-t. Liu, L.-p. Feng, and N. Li, Effect of temperature on thermal properties of monolayer MoS₂ sheet, *J. Alloys Compd.* **622**, 777 (2015).
- [18] W. Li, J. Carrete, and N. Mingo, Thermal conductivity and phonon linewidths of monolayer MoS₂ from first principles, *Appl. Phys. Lett.* **103**, 253103 (2013).
- [19] X. Gu and R. Yang, Phonon transport in single-layer transition metal dichalcogenides: A first-principles study, *Appl. Phys. Lett.* **105**, 131903 (2014).
- [20] A. N. Gandi and U. Schwingenschlöggl, Thermal conductivity of bulk and monolayer MoS₂, *Europhys. Lett.* **113**, 36002 (2016).
- [21] A. Cepellotti, G. Fugallo, L. Paulatto, M. Lazzeri, F. Mauri, and N. Marzari, Phonon hydrodynamics in two-dimensional materials, *Nature Commun.* **6**, 6400 (2015).
- [22] D. O. Lindroth and P. Erhart, Thermal transport in van der waals solids from first-principles calculations, *Phys. Rev. B* **94**, 115205 (2016).
- [23] A. Kandemir, H. Yapicioglu, A. Kinaci, T. Çağın, and C. Sevik, Thermal transport properties of MoS₂ and MoSe₂ monolayers, *Nanotechnol.* **27**, 055703 (2016).
- [24] M. K. Gupta, S. Kumar, R. Mittal, S. K. Mishra, S. Rols, O. Delaire, A. Thamizhavel, P. U. Sastry, and S. L. Chaplot, Distinct anharmonic characteristics of phonons driven lattice thermal conductivity and thermal expansion in bulk MoSe₂ and WSe₂, *J. Mater. Chem. A* **11**, 21864 (2023).
- [25] P. Hohenberg and W. Kohn, Inhomogeneous electron gas, *Phys. Rev.* **136**, B864 (1964).
- [26] W. Kohn and L. J. Sham, Self-consistent equations including exchange and correlation effects, *Phys. Rev.* **140**, A1133 (1965).
- [27] J. M. Soler, E. Artacho, J. D. Gale, A. García, J. Junquera, P. Ordejón, and D. Sánchez-Portal, The SIESTA method for *ab initio* order- N materials simulation, *J. Phys.: Condens. Matter* **14**, 2745 (2002).
- [28] A. García, N. Papior, A. Akhtar, E. Artacho, V. Blum, E. Bosoni, P. Brandimarte, M. Brandbyge, J. I. Cerdá, F. Corsetti *et al.*, SIESTA: Recent developments and applications, *J. Chem. Phys.* **152**, 204108 (2020).
- [29] F. Knoop, N. Shulumba, A. Castellano, J. P. A. Batista, R. Farris, M. J. Verstraete, M. Heine, D. Broido, D. S. Kim, J. Klarbring, I. A. Abrikosov, S. I. Simak, and O. Hellman, Tdep: Temperature dependent effective potentials, *J. Open Source Software* **9**, 6150 (2024).
- [30] O. Hellman, I. A. Abrikosov, and S. I. Simak, Lattice dynamics of anharmonic solids from first principles, *Phys. Rev. B* **84**, 180301(R) (2011).
- [31] O. Hellman, P. Steneteg, I. A. Abrikosov, and S. I. Simak, Temperature dependent effective potential method for accurate free energy calculations of solids, *Phys. Rev. B* **87**, 104111 (2013).
- [32] A. Jain, S. P. Ong, G. Hautier, W. Chen, W. D. Richards, S. Dacek, S. Cholia, D. Gunter, D. Skinner, G. Ceder, and K. A. Persson, Commentary: The Materials Project: A materials genome approach to accelerating materials innovation, *APL Mater.* **1**, 011002 (2013).
- [33] J. P. Perdew, K. Burke, and M. Ernzerhof, Generalized gradient approximation made simple, *Phys. Rev. Lett.* **77**, 3865 (1996).

- [34] K. Lee, É. D. Murray, L. Kong, B. I. Lundqvist, and D. C. Langreth, Higher-accuracy van der Waals density functional, *Phys. Rev. B* **82**, 081101(R) (2010).
- [35] M. van Setten, M. Giantomassi, E. Bousquet, M. Verstraete, D. Hamann, X. Gonze, and G.-M. Rignanese, The PseudoDojo: Training and grading a 85 element optimized norm-conserving pseudopotential table, *Comput. Phys. Commun.* **226**, 39 (2018).
- [36] D. R. Hamann, M. Schlüter, and C. Chiang, Norm-conserving pseudopotentials, *Phys. Rev. Lett.* **43**, 1494 (1979).
- [37] A. H. Romero, E. K. U. Gross, M. J. Verstraete, and O. Hellman, Thermal conductivity in PbTe from first principles, *Phys. Rev. B* **91**, 214310 (2015).
- [38] D. S. Kim, O. Hellman, N. Shulumba, C. N. Saunders, J. Y. Y. Lin, H. L. Smith, J. E. Herriman, J. L. Niedziela, D. L. Abernathy, C. W. Li, and B. Fultz, Temperature-dependent phonon lifetimes and thermal conductivity of silicon by inelastic neutron scattering and ab initio calculations, *Phys. Rev. B* **102**, 174311 (2020).
- [39] J. Klarbring, O. Hellman, I. A. Abrikosov, and S. I. Simak, Anharmonicity and ultralow thermal conductivity in lead-free halide double perovskites, *Phys. Rev. Lett.* **125**, 045701 (2020).
- [40] D. Dangić, O. Hellman, S. Fahy, and I. Savić, The origin of the lattice thermal conductivity enhancement at the ferroelectric phase transition in GeTe, *npj Comput. Mater.* **7**, 57 (2021).
- [41] D. Saleta Reig, S. Varghese, R. Farris, A. Block, J. D. Mehew, O. Hellman, P. Woźniak, M. Sledzinska, A. El Sachat, E. Chávez-Zñgel, S. O. Valenzuela, N. F. van Hulst, P. Ordejón, Z. Zanolli, C. M. Sotomayor Torres, M. J. Verstraete, and K.-J. Tielrooij, Unraveling heat transport and dissipation in suspended MoSe₂ from bulk to monolayer, *Adv. Mater.* **34**, 2108352 (2022).
- [42] I. Errea, M. Calandra, and F. Mauri, Anharmonic free energies and phonon dispersions from the stochastic self-consistent harmonic approximation: Application to platinum and palladium hydrides, *Phys. Rev. B* **89**, 064302 (2014).
- [43] S. Y. Hu, Y. C. Lee, J. L. Shen, K. W. Chen, and Y. S. Huang, Urbach tail in the absorption spectra of 2H-WSe₂ layered crystals, *Phys. Status Solidi (a)* **204**, 2389 (2007).
- [44] S. Alam, A. G. Gokhale, and A. Jain, Revisiting thermal transport in single-layer graphene: On the applicability of thermal snapshot interatomic force constant extraction methodology for layered materials, *J. Appl. Phys.* **133**, 215102 (2023).
- [45] K. Esfarjani, G. Chen, and H. T. Stokes, Heat transport in silicon from first-principles calculations, *Phys. Rev. B* **84**, 085204 (2011).
- [46] X. Wu, V. Varshney, J. Lee, Y. Pang, A. K. Roy, and T. Luo, How to characterize thermal transport capability of 2D materials fairly?—sheet thermal conductance and the choice of thickness, *Chem. Phys. Lett.* **669**, 233 (2017).
- [47] A. Molina-Sánchez and L. Wirtz, Phonons in single-layer and few-layer MoS₂ and WS₂, *Phys. Rev. B* **84**, 155413 (2011).
- [48] A. Ward and D. A. Broido, Intrinsic phonon relaxation times from first-principles studies of the thermal conductivities of Si and Ge, *Phys. Rev. B* **81**, 085205 (2010).
- [49] L. Lindsay, D. A. Broido, J. Carrete, N. Mingo, and T. L. Reinecke, Anomalous pressure dependence of thermal conductivities of large mass ratio compounds, *Phys. Rev. B* **91**, 121202(R) (2015).
- [50] I. M. Lifshitz, On thermal properties of chained and layered structures at low temperatures, *Zh. Éksp. Teor. Fiz.* **22**, 475 (1952).
- [51] M. I. Katsnelson and A. Fasolino, Graphene as a prototype crystalline membrane, *Acc. Chem. Res.* **46**, 97 (2013).
- [52] M. S. Green, Markoff random processes and the statistical mechanics of time-dependent phenomena. II. Irreversible processes in fluids, *J. Chem. Phys.* **22**, 398 (1954).
- [53] R. Kubo, Statistical-mechanical theory of irreversible processes. i. general theory and simple applications to magnetic and conduction problems, *J. Phys. Soc. Jpn.* **12**, 570 (1957).
- [54] P. Jiang, X. Qian, X. Gu, and R. Yang, Probing anisotropic thermal conductivity of transition metal dichalcogenides MX₂ (M = Mo, W and X = S, Se) using time-domain thermoreflectance, *Adv. Mater.* **29**, 1701068 (2017).
- [55] S. Varghese, J. D. Mehew, A. Block, D. S. Reig, P. Woźniak, R. Farris, Z. Zanolli, P. Ordejón, M. J. Verstraete, N. F. Van Hulst, and K. J. Tielrooij, A pre-time-zero spatiotemporal microscopy technique for the ultrasensitive determination of the thermal diffusivity of thin films, *Rev. Sci. Instrum.* **94**, 034903 (2023).
- [56] A. Mobaraki, C. Sevik, H. Yapicioglu, D. Çakır, and O. Gülseren, Temperature-dependent phonon spectrum of transition metal dichalcogenides calculated from the spectral energy density: Lattice thermal conductivity as an application, *Phys. Rev. B* **100**, 035402 (2019).
- [57] W.-X. Zhou and K.-Q. Chen, First-principles determination of ultralow thermal conductivity of monolayer WSe₂, *Sci. Rep.* **5**, 15070 (2015).
- [58] K. Yuan, X. Zhang, L. Li, and D. Tang, Effects of tensile strain and finite size on thermal conductivity in monolayer WSe₂, *Phys. Chem. Chem. Phys.* **21**, 468 (2019).
- [59] Z. Ding, J.-W. Jiang, Q.-X. Pei, and Y.-W. Zhang, In-plane and cross-plane thermal conductivities of molybdenum disulfide, *Nanotechnol.* **26**, 065703 (2015).
- [60] S. Kumar and U. Schwingenschlögl, Thermoelectric response of bulk and monolayer MoSe₂ and WSe₂, *Chem. Mater.* **27**, 1278 (2015).
- [61] X. Gu, B. Li, and R. Yang, Layer thickness-dependent phonon properties and thermal conductivity of MoS₂, *J. Appl. Phys.* **119**, 085106 (2016).
- [62] N. Bonini, J. Garg, and N. Marzari, Acoustic phonon lifetimes and thermal transport in free-standing and strained graphene, *Nano Lett.* **12**, 2673 (2012).
- [63] L. Pan, J. Carrete, and Z. Wang, Strain-tunable lattice thermal conductivity of the janus ptste monolayer, *J. Phys.: Condens. Matter* **34**, 015303 (2021).
- [64] B. Peng, D. Zhang, H. Zhang, H. Shao, G. Ni, Y. Zhu, and H. Zhu, The conflicting role of buckled structure in phonon transport of 2D group-IV and group-V materials, *Nanoscale* **9**, 7397 (2017).
- [65] D. Jose and A. Datta, Structures and chemical properties of silicene: Unlike graphene, *Acc. Chem. Res.* **47**, 593 (2014).
- [66] E. Scalise, M. Houssa, G. Pourtois, B. van den Broek, V. Afanas'ev, and A. Stesmans, Vibrational properties of silicene and germanene, *Nano Res.* **6**, 19 (2013).
- [67] J. E. Padilha and R. B. Pontes, Free-standing bilayer silicene: The effect of stacking order on the structural, electronic, and transport properties, *J. Phys. Chem. C* **119**, 3818 (2015).

- [68] M. Barhoumi, K. Lazaar, and M. Said, DFT study of the electronic and vibrational properties of silicene/stanene heterobilayer, *Physica E* **111**, 127 (2019).
- [69] C. Qian and Z. Li, Multilayer silicene: Structure, electronics, and mechanical property, *Comput. Mater. Sci.* **172**, 109354 (2020).
- [70] H. Xie, M. Hu, and H. Bao, Thermal conductivity of silicene from first-principles, *Appl. Phys. Lett.* **104**, 131906 (2014).
- [71] T. Feng and X. Ruan, Quantum mechanical prediction of four-phonon scattering rates and reduced thermal conductivity of solids, *Phys. Rev. B* **93**, 045202 (2016).
- [72] T. Feng and X. Ruan, Four-phonon scattering reduces intrinsic thermal conductivity of graphene and the contributions from flexural phonons, *Phys. Rev. B* **97**, 045202 (2018).
- [73] A. G. Gokhale, D. Visaria, and A. Jain, Cross-plane thermal transport in mos_2 , *Phys. Rev. B* **104**, 115403 (2021).
- [74] S. Chaudhuri, A. Bhattacharya, A. K. Das, G. P. Das, and B. N. Dev, Strain driven anomalous anisotropic enhancement in the thermoelectric performance of monolayer MoSe_2 , *Appl. Surf. Sci.* **626**, 157139 (2023).
- [75] A. Sood, F. Xiong, S. Chen, R. Cheaito, F. Lian, M. Asheghi, Y. Cui, D. Donadio, K. E. Goodson, and E. Pop, Quasi-ballistic thermal transport across MoS_2 thin films, *Nano Lett.* **19**, 2434 (2019).